Pertanika J. Sci. & Technol. 31 (6): 3139 - 3155 (2023)

PERTANIKA JOURNALS

SCIENCE & TECHNOLOGY

Journal homepage: http://www.pertanika.upm.edu.my/

Numerical Investigation on the Distribution of Pressure Coefficients of Modified Building Shapes

Siti Rohani Mohd Isdris[1], Shaharudin Shah Zaini[1]*, Mohammad Hafifi Hafiz Ishaik[2], Mohammad Sharizal Abdul Aziz[3] and Noorhazlinda Abd Rahman[1]

[1]*School of Civil Engineering, Universiti Sains Malaysia, 14300 USM, Nibong Tebal, Pulau Pinang, Malaysia*
[2]*School of Aerospace Engineering, Universiti Sains Malaysia, 14300 USM, Nibong Tebal, Pulau Pinang, Malaysia*
[3]*School of Mechanical Engineering, Universiti Sains Malaysia, 14300 USM, Nibong Tebal, Pulau Pinang, Malaysia*

ABSTRACT

The construction of tall buildings in urban areas has grown in number in recent years. However, architects and engineers face a variety of design challenges due to the variety of heights and shapes of new building designs. This study evaluates the impact of shape mitigation on tall buildings by applying corner modifications, such as chamfered, corner cut, plan changes with height, tapered, and setback, and combining a single modification model. The numerical simulations were carried out using Computational Fluid Dynamic (CFD) simulation with the RNG k-ε type of turbulence model. All single modifications reduced the maximum $+C_p$ and $-C_p$ better than the basic model. The corner-cut model was the most effective method for reducing the suction effect. Combining the setback, chamfering the corner, and twisting the building model at 45° modification was the most effective approach to reduce the maximum $+C_p$ in the 25–42.10% range in Face 1. Modifying a square model with the combination of setback, chamfer, and 45° rotation reduced the maximum $-C_p$, ranging from 36.9–50%. The composite 1 model and composite 2 model reduced the suction effect in the range of 15.38–33.33% in Face 3. The adoption of composite modification was insignificant in reducing the suction effect on the sidewall, where the maximum $-C_p$ was recorded to be between 3.62–5.43%.

Keywords: Aerodynamic modification, CFD, tall building, wind pressure coefficient

ARTICLE INFO

Article history:
Received: 12 December 2022
Accepted: 10 May 2023
Published: 12 October 2023

DOI: https://doi.org/10.47836/pjst.31.6.28

E-mail addresses:
ceshaharudin@usm.my (Shaharudin Shah Zaini)
sitirohani90@student.usm.my (Siti Rohani Mohd Isdris)
mhafifihafiz@usm.my (Mohammad Hafifi Hafiz Ishaik)
msharizal@usm.my (Mohammad Sharizal Abdul Aziz)
celindarahman@usm.my (Noorhazlinda Abd Rahman)
*Corresponding author

ISSN: 0128-7680
e-ISSN: 2231-8526

INTRODUCTION

Tall buildings are very common in urban areas all over the world. It is very important to study peak suctions on roofs and walls because it causes frequent damage by the peak suctions under strong wind conditions. Wind suctions at the extensions of exterior walls on corners of walls can be reduced by aerodynamic mitigation (Bitsuamlak et al., 2013). Modifying the shape of tall buildings has been proven to significantly affect crosswind loads and wind-induced responses (Irwin, 2008; Holmes, 2001; Elshaer et al., 2014; Elshaear et al., 2016). Research has been conducted to reduce excitations and improve the performance of tall buildings against wind loads. Sharma et al. (2017) studied the effect of setbacks on reducing the wind-induced response of tall buildings by three types of buildings with different setbacks and square shapes. The authors concluded that changing the cross section along the elevation through the setback could reduce the mean overturning moments along and crosswind directions. The effects and value of aerodynamic modifications, such as chamfered and recessed corners, on tall building responses were investigated by Tse et al. (2012) while maintaining the total usable floor area of the modified building form.

The study found recessed corners more effective than chamfered corners in reducing both along-wind and crosswind moments caused by buffeting and vortex-shedding excitations. Hansora et al. (2015) investigated the effect of height to width ratio of tapered-shaped tall buildings on the distribution of wind pressure coefficient around different surfaces of building models. The smallest and largest negative mean pressure coefficient on the leeward face of the building increases with increasing height/breadth (H/B) ratio. Sanyal and Dalui (2020) studied the comparison of aerodynamic coefficients of various types of Y-plans-shaped tall buildings with different types of helical, tapered, setback, and corner-modified models. Results showed that a setback building model with a rounded corner shape proved to be the most efficient among the studied models in terms of reducing wind load. In a wind tunnel test, Bandi et al. (2013) investigated aerodynamic modifications with corner cuts and helical shapes and discovered that helical buildings significantly influenced aerodynamic characteristics.

Meanwhile, Gu and Quan (2004) investigated 15 typical high-rise buildings with varying cross-sections and discovered that corner chamfers can reduce the peak value across wind base moment spectra. The review of previous work showed that most studies only focused on a single modification and effect on different types of basic models. As such, this study aims to determine the pressure distribution around various building surfaces based on single modification and changes for adopting a composite modification by using Computational Fluid Dynamics (CFD) analysis.

METHODOLOGY

This discussion explains the numerical procedures applied for the numerical simulation on tall building surfaces using ANSYS Fluent 18.0.

Shape Configuration

A total of eight building models were considered in this study. The building model was set with a height of 63 m, a base layout of 30 m x 30 m, and generated using a 1:10 scale ratio. The square model in this study is classified as a basic model with an aspect ratio H/B of 2.1 (Figure 1).

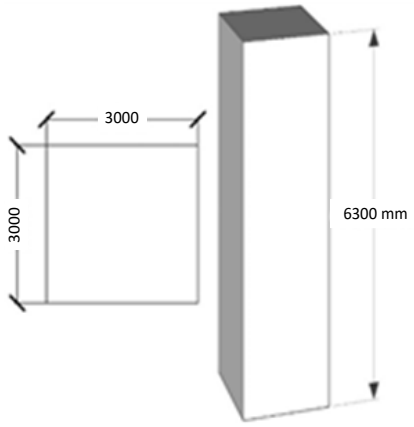

Figure 1. Basic model

The models were divided into two configurations: single modification representing a model with changes in plan area along the building height and corner modification incorporating chamfer and corner cut along four corners of the building. The chamfer and corner cut dimensions were set to be 500 mm. The detailed configuration of single modifications is shown in Figure 2.

The second type of modification includes tapering the base dimension with respect to building height, where the upper floor was reduced to 1400 mm × 1400 mm. The model with setback configuration

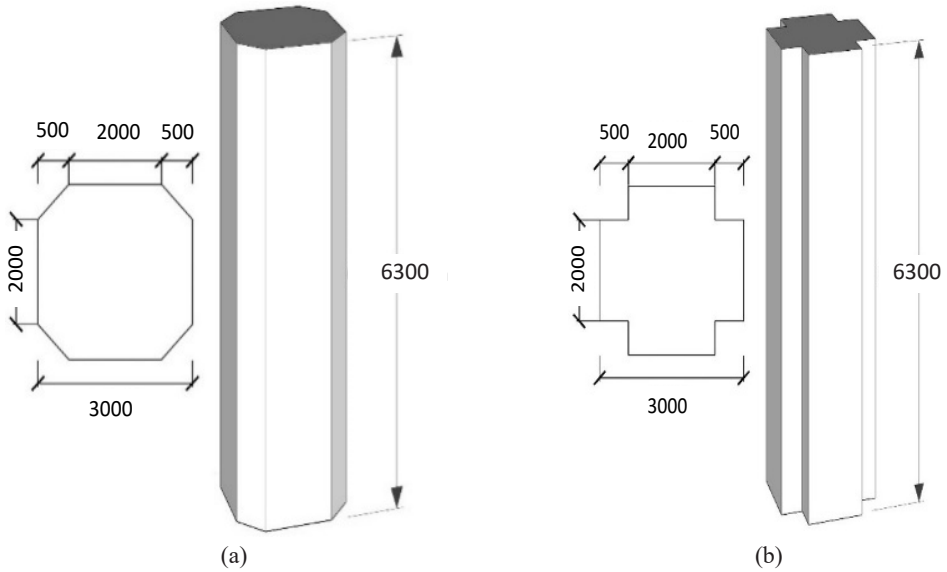

Figure 2. Single modification models (corner modification): (a) chamfered model (mm) and (b) corner cut model (mm)

was generated by reducing the plan area at every 2100 mm height. In this case, the plan dimension at 2100 mm and 4200 mm was set to be 2000 mm × 2000 mm and 1400 mm × 1400 mm (Figure 3).

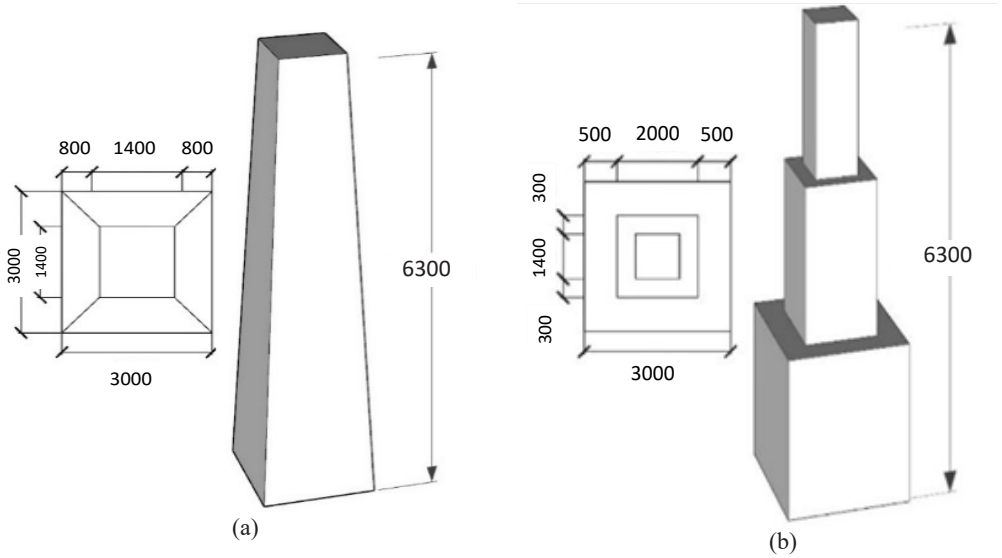

Figure 3. Single modification models (change of plan area with height): (a) tapered model (mm) and (b) corner cut model (mm)

The composite modification consists of three models with a combination of three single modifications. Figure 4 shows the details of all models under composite modification. Details of the composite models are as follows:

- Composite 1: Corner modification, setback, and rotation of 45°
- Composite 2: Corner modification, setback, and twisting of 45°
- Composite 3: Corner modification, tapered, and twisting of 45°

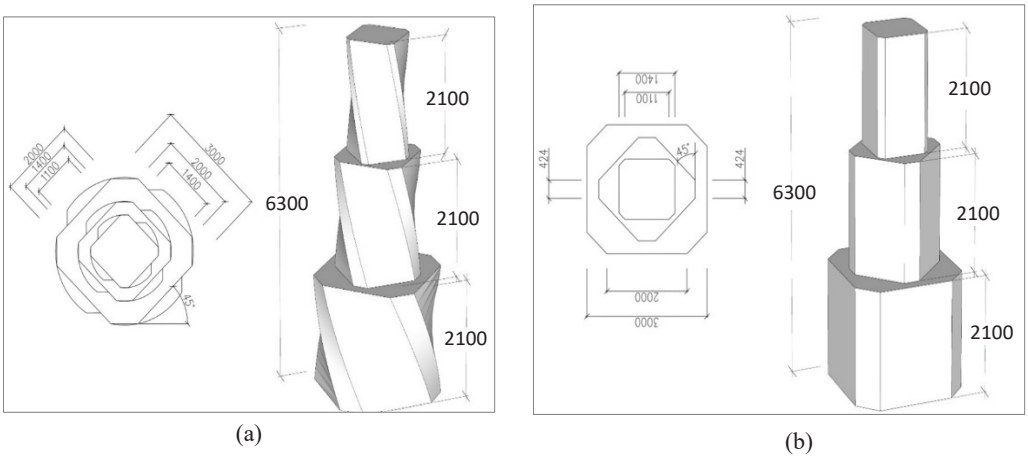

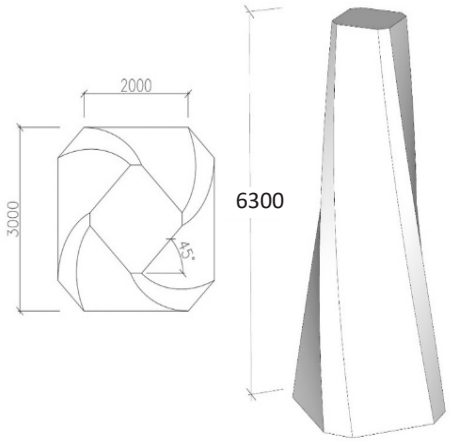

(c)

Figure 4. Composite Models (a) Composite 1 Model (mm) (b) Composite 2 Model (mm) and (c) Composite 3 Model (mm)

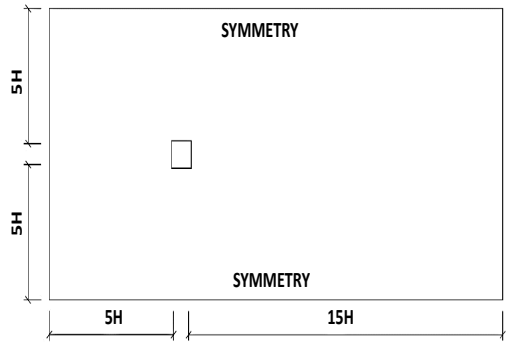

Figure 5. Plan view of the building unit in the computational domain

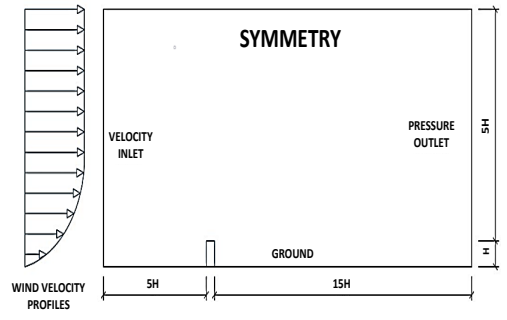

Figure 6. Side view of the building unit in the computational domain

Domain

The computational was developed based on the recommendations proposed by Franke et al. (2004). The distances were 5H from the building model to the top and the sides of the domain and 15H for the downstream length, where H was the height of the tallest building in this study. A large space was required behind the model to allow for the formation of vortices on the leeward side and to prevent wind backflow (Hajra & Dalui, 2016). The blockage ratio in the present study is in the range of 0.38%, as Tominaga et al. (2008) recommended. Figures 5 and 6 show the plan view and side view of the computational domain, respectively.

Numerical Simulation

There are several boundary conditions considered to complete this numerical modeling and simulation. The inlet boundary is specified as a velocity inlet condition. This condition specifies the velocity of flow entering the domain. The velocity inlet condition was applied using user-defined functions (UDF) developed by Deraman et al. (2018) and modified to suit the building height to define the wind profile at the inlet boundary. A pressure outlet condition is assigned at the outlet boundary with zero pressure. The sides and top boundaries of the domain are typically assigned as symmetry conditions. Meanwhile, the ground of the domain is specified as the ground where a no-slip wall condition is assigned. This condition specifies zero velocity at the wall and allows shear stresses to develop. A wall

function is assigned at these boundaries. The wind vertical profile was generated using the power law equation. The *k-ε* model was used for modeling the airflow viscosity in this study. The successful use of the *k-ε* model for analyzing the tall building model can be found in Dagnew et al. (2009), Irtaza et al. (2021), and Mou et al. (2017). Table 1 shows the overall boundary conditions used for this study.

Table 1
Boundary condition of the computational domain

Location	Boundary Condition
Inlet	Fully developed ABL inlet profile
Outlet	Pressure outlet
Top and side faces	Symmetry
Ground	Wall function

Table 2
Overall input parameters for CFD simulation in ANSYS FLUENT 18.0

Parameters	Inputs
Equation	Steady-RANS
Turbulence Model	RNG *k-ε*
Roughness height, ks	0.001 sm
Roughness constant, Cs	1.0
Power law exponent	0.0035
Mean wind speed, v	15 m/s
Pressure velocity coupling	SIMPLE algorithm
Spatial discretization for pressure and momentum	Second-order

This study used the Renormalization Group (RNG) *k-ε* model, a Reynolds Averaged Navier Stokes (RANS) based two equations turbulence model. The inlet velocity of flow was set to be 15 m/s based on a standard tall building model tested at two research institutions, namely City University of London and National Aeronautical Establishment, to ensure that the flow over a surface will be turbulent if Reynold's Number is more than 10^5 (Khan & Roy, 2017). The power-law profile was scaled to 1/7 to represent flat terrain. Since scaled-down models were used, the roughness length was also scaled down to Z_0 = 0.035/10, as Khan and Roy (2017) recommended. Table 2 shows the input parameter used for this study.

Mesh Arrangement

Mesh quality is a very important criterion for the correctness of simulation results. Structured (hexahedral) and unstructured (tetrahedrons and prisms) are two kinds of mesh that have been widely accepted in CFD simulation (Irtaza et al., 2021). Because the geometry in this study is complex, it was impossible to have structured mesh throughout the domain. Therefore, to solve this problem, the building is placed in a rectangular prism. An unstructured mesh is generated for zones in the nesting rectangular prism, while for the zones around the nesting prism, the structured mesh is applied. Figures 7 to 9 show the mesh arrangement for the building model in this study.

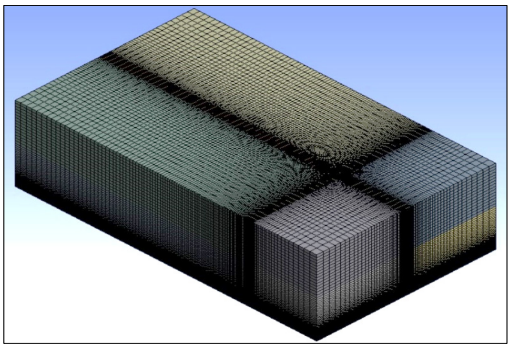

Figure 7. Isometric view showing the overall computational domain

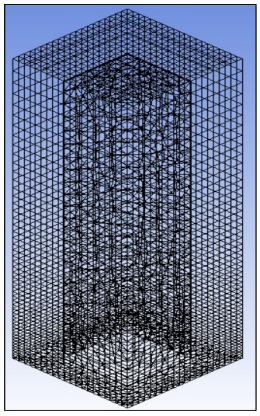

Figure 8. Zoom in, showing the model inside the domain

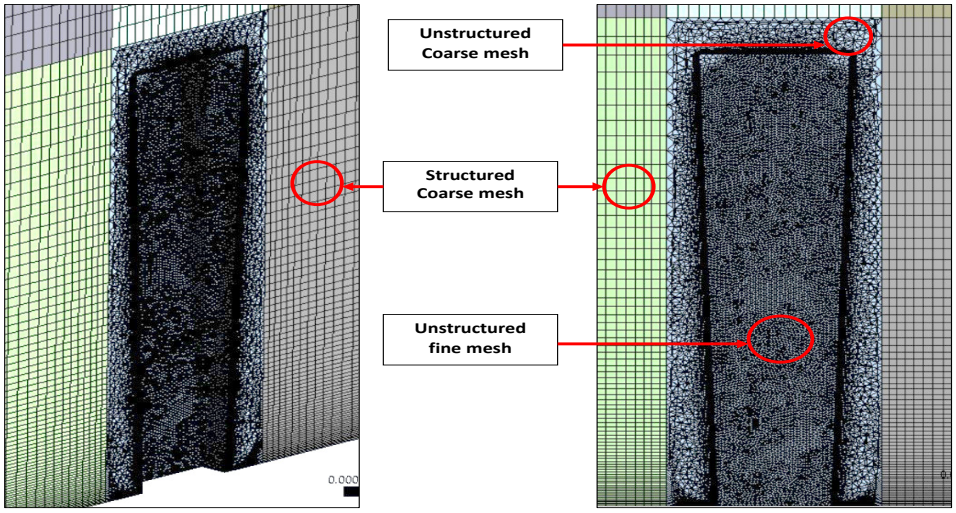

Figure 9. Cut section view

VALIDATION AND ANALYSIS

Since numerical results are affected by a range of factors, it is essential to validate the correctness of the numerical model and the precision of numerical results.

Grid Convergence Study

In a CFD analysis, the grid convergence study plays an important role in identifying the correct mesh pattern to significantly diminish the computational time and error (Bhattacharjee et al., 2021). Franke et al. (2004) recommend that at least three systematically refined grids be conducted to quantify the influence of the grid resolution for the solution. In this exercise, five different grid sizes, namely mesh 1 (Very Course), mesh 2 (Course),

mesh 3 (Medium), mesh 4 (Fine) and mesh 5 (Very Fine) were generated. The number of elements for these four grids is 239056, 402067, 567592, 727997, and 895985. In order to produce a constant increase in the number of elements, the difference in terms of number of elements between successive mesh regimes was set at 160,000. The difference between the very coarse and very fine grid schemes was calculated to be more than 3.2, as Franke et al. (2004) recommended. Figure 10 shows the result of the comparison of C_p profiles for grid sensitivity analysis. From the results, all models showed similar distribution, particularly true at the building's Face 1 and Face 3. In Face 1, the model with a fine grid scheme (mesh 5) showed the highest C_p (0.757), followed by mesh 4 (0.755), mesh 3 (0.751), mesh 2 (0.744), and mesh 1 (0.73). Tominaga et al. (2015) stated that the maximum $+C_p$ on the wall should be close to 1 due to the formation of a stagnation point. As such, mesh 5 showed the most accurate results compared to other models.

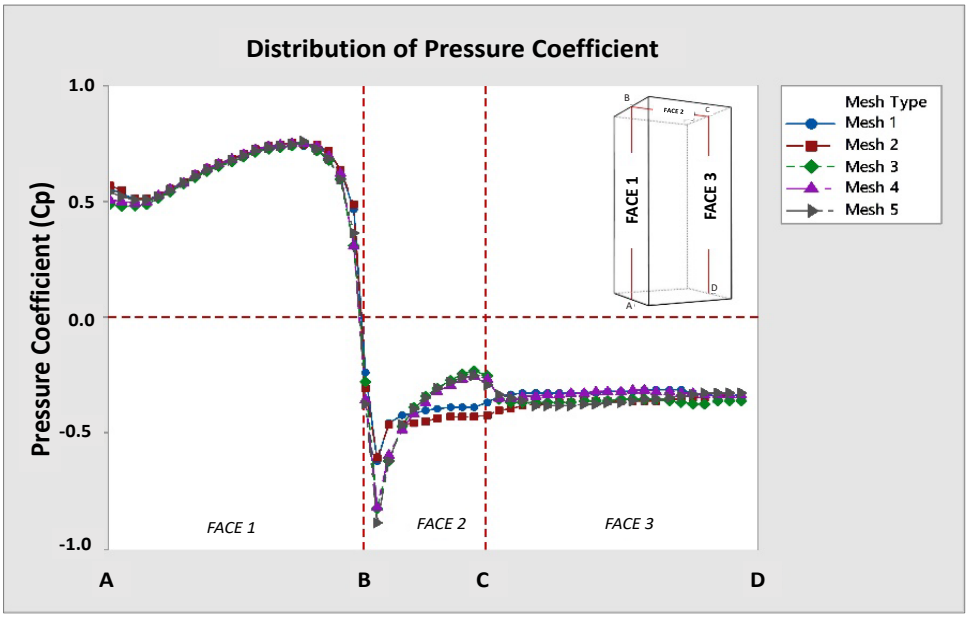

Figure 10. Comparison of *Cp* profiles for grid sensitivity analysis

The comparison of the overall computational time taken for every mesh model is shown in Figure 11. The results showed that Mesh 5 took approximately 10 hours to converge at 5000 iterations, followed by Mesh 4 (8 hours), Mesh 3 (6 hours), Mesh 2 (4 hours) and Mesh 1 (2 hours). Although Mesh 4 and Mesh showed relatively small differences in Face 2, the difference in terms of the computational time was calculated to be 2 hours. This difference is still manageable. By considering the importance of obtaining reliable results, model Mesh 5 was selected.

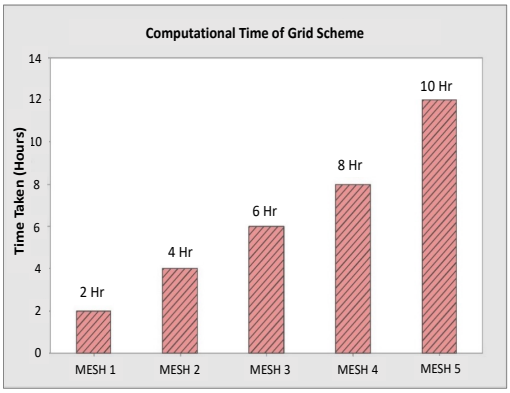

Figure 11. Comparison of time taken for every model to converge

Validation Model

The validation exercise was performed to ensure the reliability of the input parameters in ANSYS. In this case, the Commonwealth Advisory Aeronautical Council (CAARC) standard tall building model results tested by Dagnew et al. (2009) using wind tunnel test (WTT) and CFD was used (Figure 12). The validation model's Reynolds number at 3.8 x 10^5 was based on building height H and the inflow velocity U_H at z = H, as stated by Dagnew et al. (2009). Other input parameters were generated using data from other literature (Huang et al., 2009; Meng et al., 2017; Ahsan, 2014; Liu & Niu, 2016). Parameters such as air density and solid material type were assumed to suit the condition. The density of air is affected by temperature, pressure, and dew point. This study took air density and dynamic viscosity as 1.225 kg/m^3 and 1.79 x 10^{-5}, respectively. This study used the Renormalization Group (RNG) *k-ε* Model, the Reynolds Averaged Navier Stokes (RANS) based on two equations turbulence model. The inlet velocity of flow was set to be 12.7 m/s, followed by Dagnew et al. (2009).

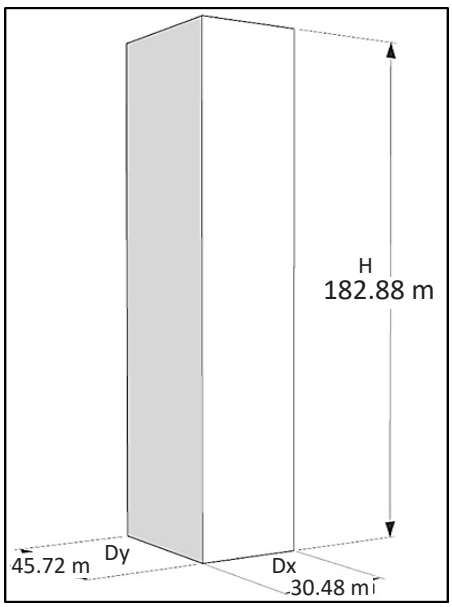

Figure 12. Isolated standard tall building

Validation Results

Figure 13 shows the overall results from WTT and CFD by Dagnew et al. (2009) and the validation model (CFD Validation) generated using ANSYS. The wind pressure coefficient in this study was measured at 2/3 of the building height. It is pointed out that wind pressure coefficients at 2H/3 of the standard model are sufficient for model calibration (Montazeri & Blocken, 2013; Huang et al., 2009). The CFD Validation agrees with CFD Dagnew and is particularly true at Surface 1. Although both CFD results cannot capture the maximum $+C_p$ in Surface 1, theoretically, the maximum $+C_p$ must be 1.0 or close to 1.0 to define the location of

the stagnation point. In addition, the validation model follows the C_p distribution pattern relatively closely compared to CFD Dagnew in Surface 2, 3, and 4. In order to verify the similarity of the C_p distribution between the CFD Validation and the results from Dagnew et al. (2009), the error measures analysis was conducted, and the summary is shown in Table 3. In this case, the error measures exercise comprises Mean Absolute Error (MAE), Normalized Absolute Error, and Root Mean Square Error (RMSE). It is worth mentioning that when the similarity is high, then the discrepancy of the overall results is low (Table 3). The CFD Validation model provides the smallest error for all the error measure analyses and possesses high similarity to the WTT test and CFD work by Dagnew et al. (2009). As such, the input parameters in the CFD analysis of the validation work are reliable.

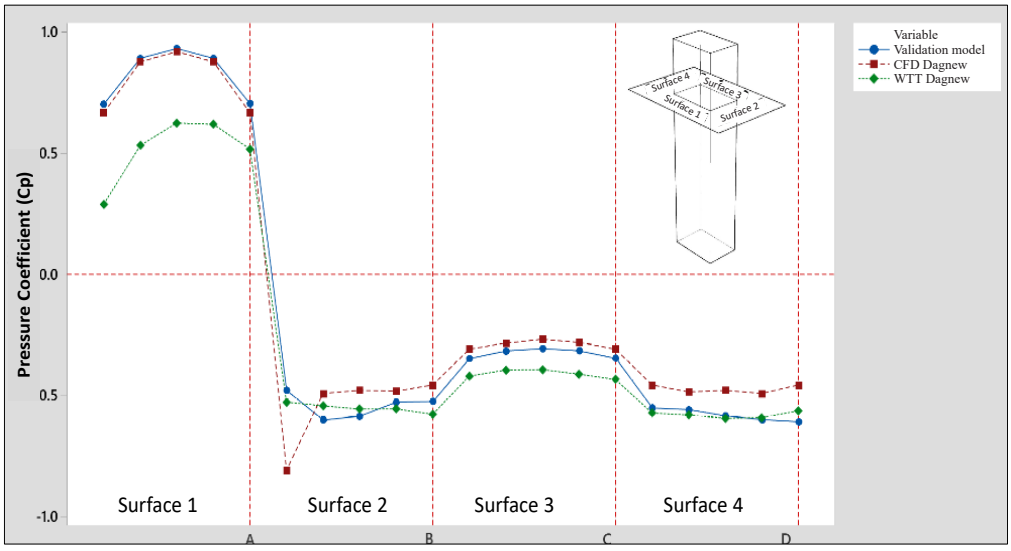

Figure 13. C_p profile between validation model, CFD Dagnew, and WTT Dagnew

Table 3
Summary of error measures

Error Measure	WTT Dagnew	
	CFD Dagnew	CFD Validation
MAE	0.158	0.124
NAE	0.306	0.245
RMSE	0.184	0.183

RESULTS AND DISCUSSION

The C_p profile for the basic model with overall single-corner modification is shown in Figure 14. For the basic model, the maximum $+C_p$ is located at approximately two-thirds of the building height for the basic model with a value of +0.76. A similar pattern was also observed in the work of Tominaga et al. (2008) and Richard et al. (2007). Meanwhile, the distribution pattern of the pressure coefficient for the Chamfered and Corner cut models is similar to the basic model. In this case, the maximum $+C_p$ and

-C_p were recorded to be +0.56 and -0.51 for chamfered and +0.6 and -0.46 for the corner cut model. By introducing chamfered corner, the reduction in terms of the overall C_p for Face 1 (windward), Face 2 (roof), and Face 3 (leeward) was calculated to be approximately 5.43% to 44.56% and 18.5% to 50.0%, respectively. The model with the chamfered corner exhibits the lowest +C_p across Face 1, and the corner-cut model generates the lowest suction along most of the surface of the roof.

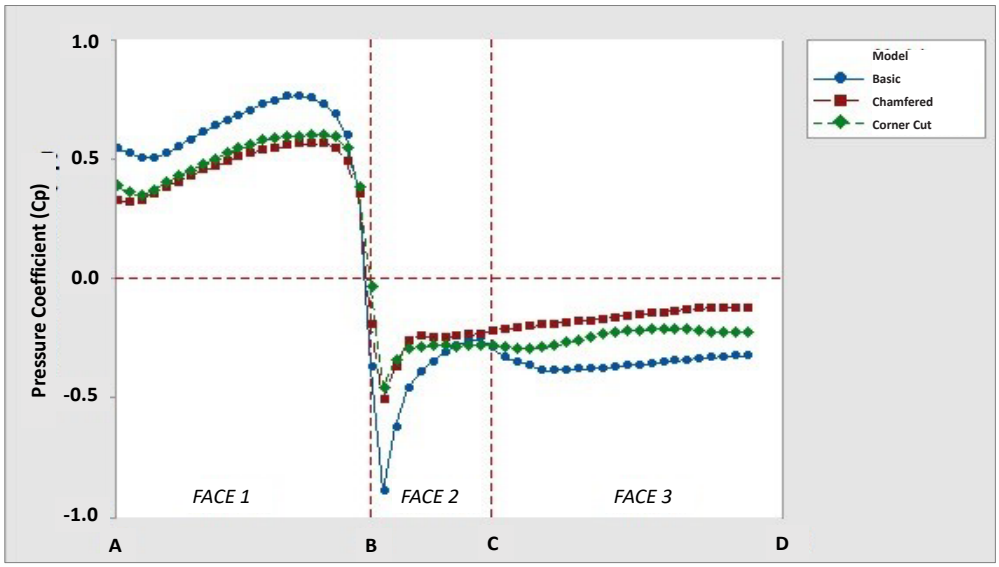

Figure 14. C_p profile for overall single modification (corner modification)

Figure 15 shows the overall comparison distribution in terms of pressure coefficient for the basic, setback, and tapered models. The pattern of the C_p distribution shows a similar trend to the basic models. However, for the setback model, a slight drop in the C_p values occurs at every setback location (refer to the red circles). The maximum +C_p was formed in Face 1, and the value was recorded to be +0.65 and +0.75 for the tapered and setback models, respectively. Moreover, the maximum -C_p for the tapered and setback models was found to be -0.49 and -0.72, respectively. The -C_p values in Face 3 are almost constant with no noticeable fluctuation for the tapered model, whereas a slight fluctuation in the pattern along Face 3 is shown for the setback model at the boundary between setbacks. As such, the modification made to the models by changing the plan area with height resulted in an efficient reduction of suction for both models.

Figure 16 shows the pressure contour on the overall surfaces of the building models. All models develop -C_p at the side wall. The reduction of -C_p at the side walls of single corner modification can be associated with sharp corners on the basic model. Sharp corners can produce stronger vortices than the models with modified corners (Holmes, 2015). In terms

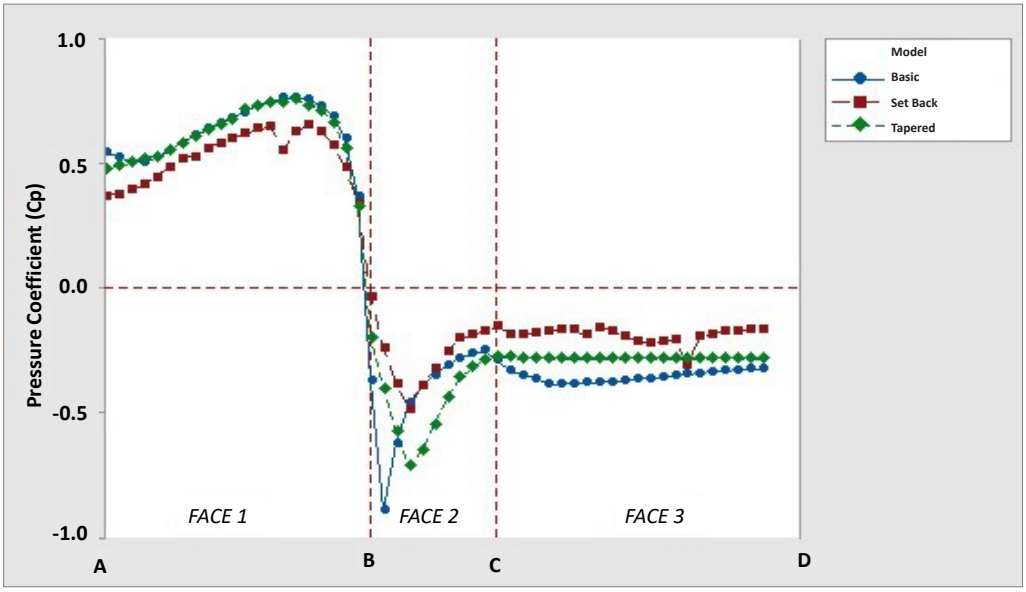

Figure 15. C_p profile for overall single modification (changes in plan area with respect to building height)

of suction, the introduction of corner cuts is more efficient than chamfering the corner. It is due to buildings with sharp corners induced strong vortices or vortex shedding. As such, to break up the vortices and lose their coherence, softening to the sharp edges must be made by introducing corner cut or chamfer, as Irwin (2008) reported. In addition, the modification of the plan area with respect to height was found to reduce the suction effect. The maximum suction for the basic model (-0.92) is reduced to -0.79 and -0.65, as shown by the tapered and setback models. Moreover, the setback model performs better than the tapered model in reducing the suction at the side wall due to the reduction of the kinetic energy in Face 1 that was prolonged to the side walls and weakened the wake region.

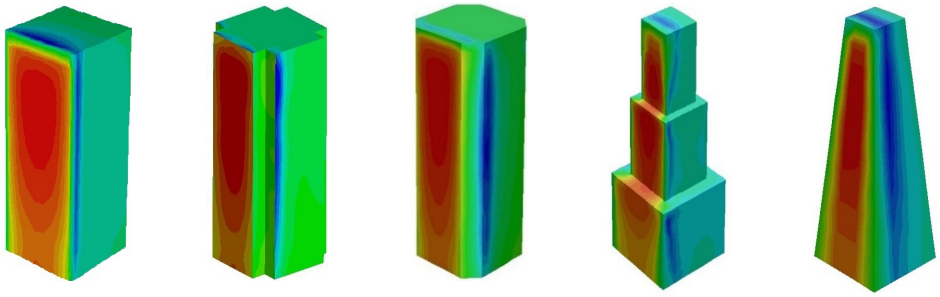

(a) (b) (c) (d) (e)

Figure 16. Pressure contour on the overall surfaces of the building models (a) Basic, (b) Corner Cut, (c) Chamfered, (d) Setback, and (e) Tapered

Figure 17 shows the overall C_p profile for composite models and basic models. The maximum $+C_p$ recorded in Face 1 for the composite 1 model is +0.57. On the other hand, in Face 2, the maximum $-C_p$ was found to be -0.46. The C_p distribution shows slight fluctuation in Face 3; the highest $-C_p$ was recorded to be approximately -0.25. The distribution pattern for the composite 1 model is similar to the setback model. It is particularly true because both models show $+C_p$ reduction at the setback locations. Meanwhile, the trend for the composite 2 model is similar to the setback model and the composite 1 model due to the relatively dominant effect of the setback feature. The maximum $+C_p$ was recorded to be +0.44. The magnitude of the pressure drop at the upper part of the setback location is larger than the lower part of the setback. On the other hand, Face 2 develops the highest $-C_p$, which is recorded to be -0.58. The $-C_p$ fluctuates and stabilizes at approximately -0.2 in Face 3. Meanwhile, unlike the composite 1 model and composite 2 model, the distribution pattern for the composite 3 model is relatively smooth without any significant drops in Face 1 and Face 3. The maximum $+C_p$ for windward Face 1 was recorded to be +0.54, and the maximum $-C_p$ for windward Face 2 was recorded to be -1.08. The $-C_p$ is significantly reduced as it approaches the rear part of the roof and slightly fluctuates in Face 3. The suction effect was weakened at the lower part of Face 3, and the $-C_p$ stabilized at approximately -0.1.

From the graph shown, it clearly can be seen that, in the case of Face 1, the results showed that all composite models showed a significant reduction in the $+C_p$. The composite model 1 and composite model 3 showed almost similar magnitude in terms of $+C_p$ throughout Face 1. On the other hand, the composite model 2 was shown to produce the lowest $+C_p$ along Face 1. This phenomenon can be associated with the effectiveness of combining chamfered, setback, and twisting to the basic model. On the other contrary, In Face 2, the composite 1 model showed the lowest $-C_p$ (thus the suction effect) compared to other models. By studying the formation of the composite 1 model and comparing these features with the composite 2 model and composite 3 model, rotating the model at 45° and introducing setbacks were shown to be effective in reducing the $-C_p$. The kinetic energy of the airflow for the composite 2 model was reduced due to the presence of a setback where the kinetic energy was further reduced with the wind reduction drag due to the presence of twisted surfaces.

Despite significantly reducing kinetic energy (low $+C_p$), the condition was not prolonged in Face 2. This phenomenon is because the separation and reattachment of airflow did not interfere with the reverse flow direction generated by the vortex in Face 3. It is evident that in the composite 1 model, although having higher kinetic energy (high $+C_p$), the condition was significantly reduced when the separated flow encountered the reverse flow from the generated vortex at the upper level. Interestingly, the composite 3 model exhibited the highest $-C_p$ in Face 2, and the value exceeded the basic model.

Although the kinetic energy in the composite 3 model was shown to be relatively similar to the composite 1 model, the suction effect in Face 2 was more dominant due to the fact that the axis of the vortex at the upper level was found to be relatively far from the suction region in Face 2. Generally, throughout Face 3, the composite models showed lower -C_p values compared to the basic model.

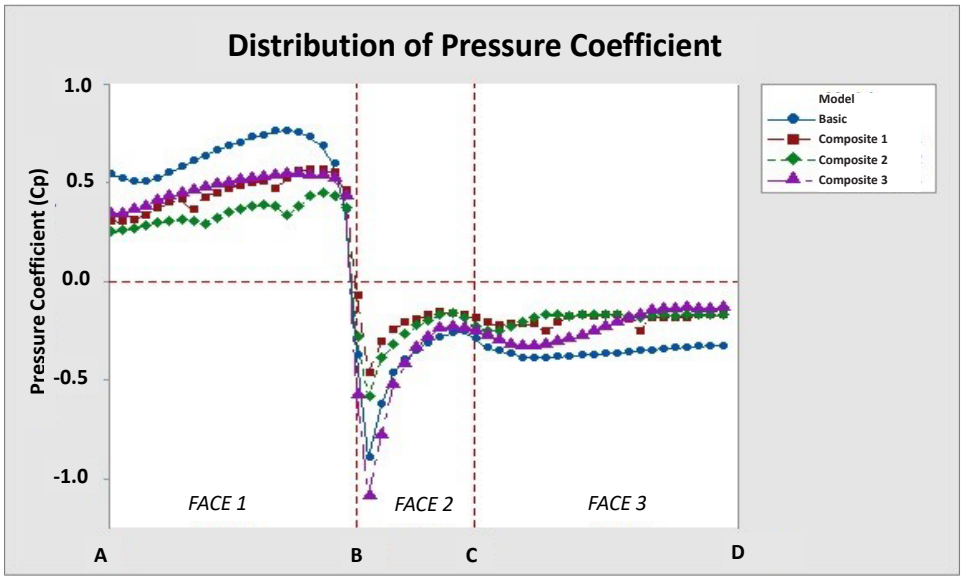

Figure 17. C_p profile for basic and overall composite modification

The pressure contour on the side of the building models is shown in Figure 18 for the composite 1 model, composite 2 model, and composite 3 model. The side surface for all models generates both +C_p and -C_p. The maximum suction exhibited from the side of the building model is shown in the composite 3 model (-1.08), followed by composite 2 model (-0.89) and composite 1 model (-0.9). In this case, only the composite 3 model exceeded the maximum suction of the basic model (-0.92). The difference was calculated to be 17.39%. In addition, the combination of setback, chamfer, and 45° rotation in composite model 1 can reduce the maximum -C_p approximately half of the value exhibited by the basic model. For composite modifications, the formation of the highest suction only occupies a relatively small area on the surface and close to the edge of the corner surface. Especially for the composite 2 model and composite 3 model, the area exhibiting a high suction effect was concentrated at the upper level of the building.

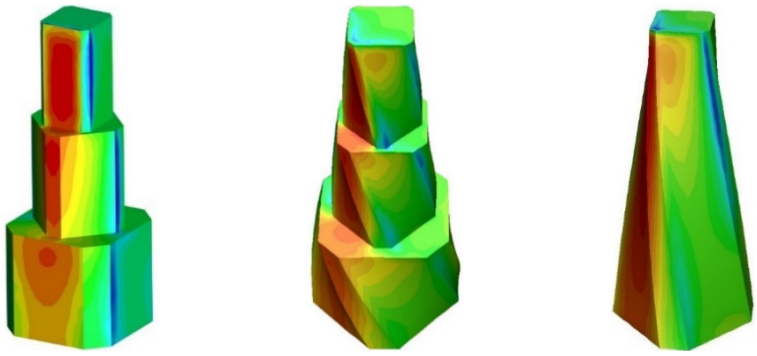

(a) (b) (c)

Figure 18. Pressure contour on the overall surfaces of the building models (a) composite 1, (b) composite 2, (c) composite 3

CONCLUSION

All models subjected to single modification performed better than the basic model in reducing the maximum $+C_p$ and $-C_p$. In terms of suction, a corner cut was shown to be more efficient than a chamfer. The setback model is more effective in reducing suction than the basic and tapered model. When comparing the composite 1 model with the composite 2 model in Face 1, twisting was more efficient in reducing the $+C_p$ than rotation. For the composite 2 and the composite 3 models, a tapered configuration was more efficient than setting the building with setbacks. Meanwhile, when comparing the composite 1 model to the composite 2 model and the composite 3 model, it was discovered that rotating the model at 45° and introducing setbacks effectively lowered the $-C_p$. Choosing an efficient geometry modification for high-rise structures can help mitigate aerodynamic concerns, particularly in pressure distribution on the building surfaces. This study only focuses on the use of RNG k-ε. Other turbulence models, such as Large Eddy Simulation (LES) and Detached Eddy Simulation, can be explored with wind tunnel tests on other complex building shapes.

ACKNOWLEDGEMENT

The authors express their gratitude and appreciation to the Universiti Sains Malaysia for providing all the required facilities**.**

REFERENCES

Ahsan, M. (2014). Numerical analysis of friction factor for a fully developed turbulent flow using k-ε turbulent model with enhanced wall treatment. *Beni-Suef University Journal of Basic and Applied Science*, *3*(4), 269-277. https://doi.org/10.1016/j.bjbas.2014.12.001

Bandi, E. K., Tamura, Y., Yoshida, A., Kim, Y. C., & Yang, Q. S. (2013). Experimental investigation on aerodynamic characteristics of various triangular section highrise buildings. *Journal of Wind Engineering and Industrial Aerodynamics*, *122*, 60-68. https://doi.org/10.1016/j.jweia.2013.07.002

Bitsuamlak, G. T., Warsido, W., Ledesma, E., & Chowdhury, A. G. (2013). Aerodynamic mitigation of roof and wall Corner suctions using simple architectural elements. *Journal of Engineering Mechanics*, *139*(3), 396-408. https://doi:10.1061/(ASCE)EM.1943-7889.0000505

Bhattacharjee, S., Banerjee, S., Majumdar, S., Saptaparni, S. G., Dey, A., & Sanyal, P. (2021). Effects of irregularity on a butterfly plan-shaped tall building under wind load. *Journal of The Institution of Engineers (India): Series A*, *102*, 451-467. https://doi.org/10.1007/s40030-021-00511-6

Dagnew, A. K., Bitsuamalk, G. T., & Merrick, R. (2009, June 22-26). A Computational evaluation of wind pressures on tall buildings using LES. In *11th Americas Conference on Wind Engineering* (pp 1-17). San Juan, Puerto Rico. https://doi.org/10.12989/was.2014.18.5.567

Deraman, S. N. C., Majid, T. A., Zaini, S. S., Yahya, W. N. W., Abdullah, J., & Ismail, M. A. (2018). Enhancement of CFD validation exercise along the roof profile of a low-rise building. In *IOP Conference Series: Earth and Environmental Science* (Vol. 140, No. 1, p. 012004). IOP Publishing. https://doi.org/10.1088/1755-1315/140/1/012004

Elshaer, A., Bitsuamlak, G., & Damatty, A. E. (2014, June 1-4). Wind load reductions due to building corner modifications. In *22nd Annual conference of the CFD society of Canada* (pp. 1-5). Toronto, Canada.

Elshaer, A., Bitsuamlak, G., & El Damatty, A. (2016, June 7-11). Aerodynamic shape optimization of tall buildings using twisting and corner modifications. In *8th International Colloquium on Bluff Body Aerodynamics and Applications Northeastern University* (pp. 1-8). Boston, MA, USA.

Franke, J., Hirsch, C., Jensen, A. G., Krus, H. W., Schatzmann, M., Westbury, P. S., Miles, S. D., Wisse, J. A., & Wright, N. G. (2004, May 5-7). Recommendations on the use of CFD in wind engineering. In *Proceedings of the International Conference on Urban Wind Engineering and Building Aerodynamics* (pp. C.1.1-C1.11). von Karman Institute, Sint-Genesius-Rode, Belgium.

Gu, M., & Quan, Y. (2004). Across wind loads of typical tall buildings. *Journal of Wind Engineering and Industrial Aerodynamics*, *92*(13), 1147-1165. https://doi.org/10.1016/j.jweia.2004.06.004

Hajra, S., & Dalui, S. K. (2016). Wind interference effect on an octagonal plan shaped tall building due to square plan shaped tall buildings. *Jordan Journal of Civil Engineering*, *10*(4), 462-479. https://doi.org/10.1007/s40091-016-0115

Hansora, A. G., Gehlot, K. P., & Nimodiya, P. N. (2015). Numerical analysis of wind loads on tapered shape tall buildings. *International Journal of Science Technology & Engineering*, *1*(11), 92-97.

Holmes, J. D. (2001). *Wind loading of structures: Wind Loading of Structures* (1st ed.). CRC Press. https://doi.org/10.4324/9780203301647

Holmes, J. D. (2015). *Wind loading of structures* (3rd ed.). CRC Press. https://doi.org/10.1201/b18029

Huang, S., Li, Q. S., & Xu, S. (2009). Numerical evaluation of wind effects on a tall steel building by CFD. *Journal of Construction Steel Research*, *63*(5), 612-627 https://doi.org/10.1016/j.jcsr.2006.06.033

Irwin, P. A. (2008). Bluff body aerodynamics in wind engineering. *Journal of Wind Engineering and Industrial Aerodynamics*, *96*, 701-712. https://doi.org/10.1016/j.jweia.2007.06.008

Irtaza H., Agarwal, A., & Shahab K. (2021). Comparison of aerodynamic loads on prismatic and twisted tall buildings using computational fluid dynamics. *Journal of The Institution of Engineers (India): Series C*, *102*, 635-650. https://doi.org/10.1007/s40032-021-00694-8

Khan, M. M., & Roy, A. K. (2017). CFD simulation of wind effects on industrial RCC chimney in civil engineering Conference-Innovation for sustainability. *International Journal of Civil Engineering and Technology (IJCIET)*, *8*(1), 1008-1020.

Liu, J., & Niu, J. (2016). CFD Simulation of the wind environment around an isolated high-rise building: An evaluation os SRANS, LES and DES models. *Journal of Building and Enviroment*, *96*, 91-106.

Meng, F. Q., He, B. J., Zhu, J., Zhao D. X., Darko, A., & Zhao, Z. Q., (2017). Sensitivity analysis of wind pressure coefficients on CAARC standard tall buildings in CFD Simulations. *Journal of Building Engineering*, *16*, 146-158. https://doi.org/10.1016/j.jobe.2018.01.004

Montazeri, H., & Blocken B. (2013). CFD simulation of wind induced pressure coefficient on buildings with and without balconies: validation and sensitivity analysis. *Journal of Building and Environtment*, *60*, 137-149. https://doi.org/10.1016/j.buildenv.2012.11.012

Mou, B., He, B. J., Zhao, D. X., & Chau K. W., (2017). Numerical simulation of the effects of building dimensional variation on wind pressure distribution. *Engineering Applications of Computational Fluid Mechanics*, *11*, 293-309. https://doi.org/10.1080/19942060.2017.1281845

Richards, P. J., Hoxey, R. P., Connell, B. D., & Lander, D. P. (2007). Wind-tunnel modelling of the Silsoe Cube. *Journal of Wind Engineering and Industrial Aerodynamics*, *95*, 1384-1399. https://doi.org/10.1016/j.jweia.2007.02.005

Sanyal, P., & Dalui, S. K. (2020). Comparison of aerodynamic coefficients of various types of Y-plan shaped tall buildings. *Asian Journal Civil Engineering*, *21*(7), 1109-1127. https://doi.10.1007/s42107-018-0018-3

Sharma, A., Mittal, H., & Gairola, A. (2017, December 3-7). Investigation of aerodynamic forces on highrise buildings with setback modification. In *9th Asia-Pacific Conference, Wind Engineering* (pp. 1-4). Auckland New Zealand.

Tse, K. T., Hitchcock, P. A., Kwok, K. C. S., Thepmongkorn, S., & Chan, C. M. (2012). Economic perspectives of aerodynamic treatments of square tall buildings. *Journal of Wind Engineering and Industrial Aerodynamics*, *97*(9-10), 455-467. https://doi:10.1016/J.JWEIA.2009.07.005

Tominaga, Y., Mochida, A., Yoshie, R., Kataoka, H., Nozu, T., Yoshikawa, M., & Shirasawa, T. (2008). AIJ guidelines for practical applications of CFD to pedestrian wind environment around buildings. *Journal of Wind Engineering and Industrial Aerodynamics*, *96*(10-11), 1749-1761. https://doi.org/10.1016/j.jweia.2008.02.058

Tominaga, Y. (2015). Air flow around isolated gable-roof buildings with different roof pitches: Wind tunnel experiments and CFD simulations. *Building and Environments*, *84*, 204-213. https://doi.org/10.1016/j.buildenv.2014.11.012